Control Technologies in Distributed Generation System Based on Renewable Energy

Jie Wu [1] Sizhe Chen [1] Jun Zeng [1] Lamei Gao [1]

Abstract – Greats efforts have been done to distributed renewable energy (RE) power system in latest years. This paper summarizes the research achievements of New Energy Research Center (a research center in Electric Power College, South China University of Technology) in distributed RE power system. The paper is mainly divided into three parts, including wind energy generation, photovoltaic generation and energy management system. Firstly, the wind energy generation control technologies is presented in variable speed constant frequency, maximum wind power capture, power decoupled control, pitch control, low voltage ride through, and grid synchronization. Secondly, the photovoltaic generation control technologies is introduced including photovoltaic maximum power point tracing, configuration and optimization of photovoltaic array and grid-connected converter. Lastly, the energy management system is proposed as the super manage layer to hybrid REs, which including wind speed forecast, integrative evaluate to power quality, power quality analytical instrument and the construction of energy management system based on multi-agent technology.

Keywords – Distributed generation, Wind energy generation, Photovoltaic generation, Energy management system

I. INTRODUCTION

With the gradual depletion of fossil energy resources and the increasingly serious issue of environmental pollution, great concern is paid to the development of renewable energy (RE), such as wind and solar energy. The development of distributed RE power system play more and more important role in traditional power system as a useful complement to the grid. It is a good way to reduce energy consumption, improve flexibility and reliability of power system.

The distributed power system generally refers to relatively small-scale power generation system (typically 50 MW or less). It is mainly made up of RE, including bio-energy power generation, solar power, wind energy and small-scale gas turbine power generation and energy storage devices. It is always located at the user-site nearly, which can be connected to power grid or isolated operated as shown in Fig.1.

In the latest years, great efforts have been done in distributed RE power system at the New Energy Research Center of South China University of Technology. Nowadays, Guangdong Key Laboratory of Clean Energy Technology is built based on these research achievements.

This paper has been published in PESA09 Conference and has been selected to be published in this APEJ issue.

[1]College of Electric Power, South China University of Technology,Guangzhou,China,510640E-mail:epjiewu@scut.edu.cn

This paper introduces the research results of NERC, which focuses on the complex dynamic control technologies in distributed RE power system. Some simple or mature control technologies are out of the scope of this article, such as battery charging, braking and yawing.

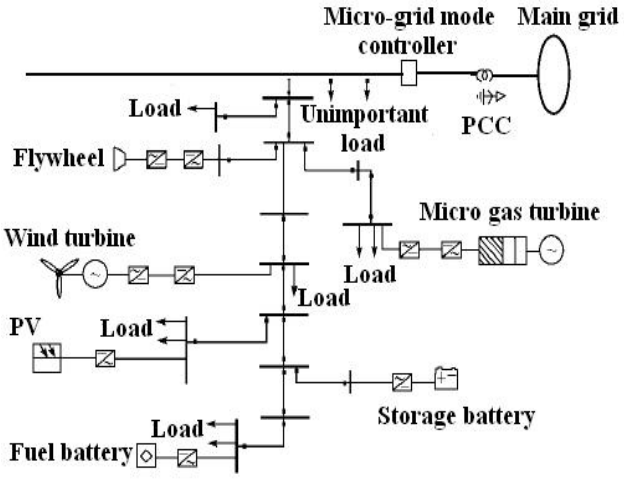

Fig. 1 Structure of distributed generation system

II. CONTROL TECHNOLOGIES IN WIND ENERGY GENERATION

A. *Variable speed constant frequency*

In order to improve the efficiency and power quality of wind energy conversion system (WECS), achieve variable speed constant frequency (VSCF) generation, and get rid of the slip ring maintenance in conventional doubly-fed induction generation (DFIG), a brushless doubly-fed machine (BDFM) is designed and manufactured [2]. The structure of BDFM is shown in Fig.2. There are two windings in the stator: power winding and control winding. The pole pair number of power winding p_p is four, and the pole pair number of control winding p_c is one. The relations among power winding frequency f_p, control winding frequency f_c and rotary frequency f_r is given as

$$f_r = \frac{f_p \pm f_c}{p_p + p_c} \tag{1}$$

Under different rotary speed, the power winding frequency can be controlled to fellow the grid frequency by adjusting the frequency of control winding exciting converter, and hence VSCF will be achieved. Fig.3 shows the voltage of the BDFM power winding under different rotary speed and load conditions. When the rotary speed changed, the power winding frequency can be keep at 50 Hz by adjusting the exciting converter frequency.

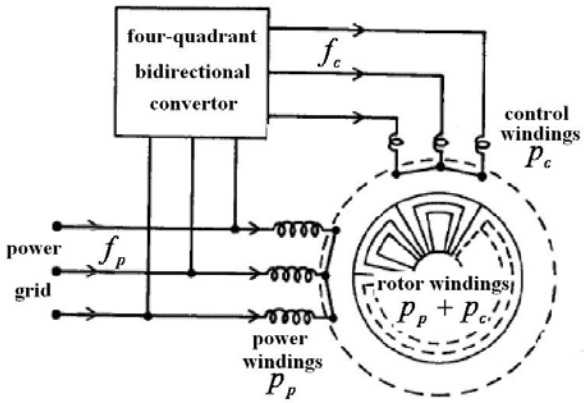

Fig.2 Structure of BDFM

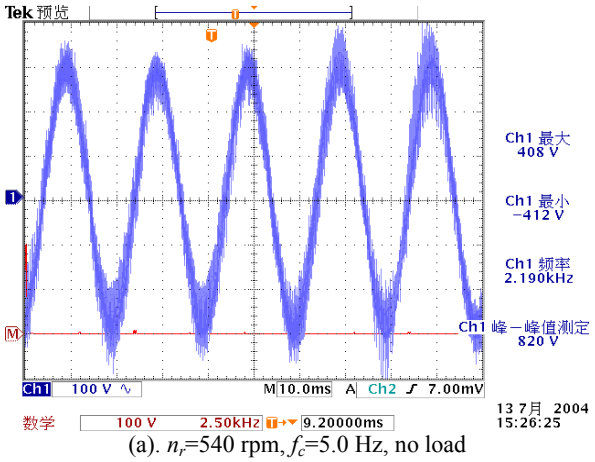

(a). n_r=540 rpm, f_c=5.0 Hz, no load

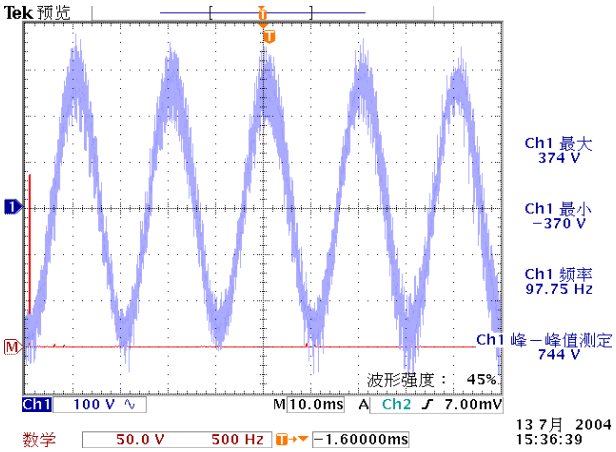

(b). n_r =540 rpm, f_c =5.0 Hz, with resistance load

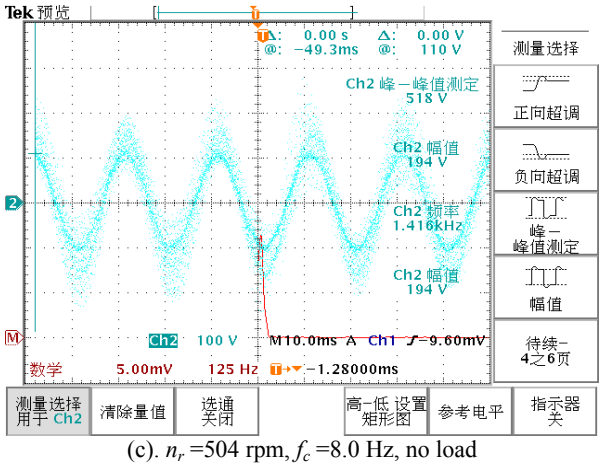

(c). n_r =504 rpm, f_c =8.0 Hz, no load

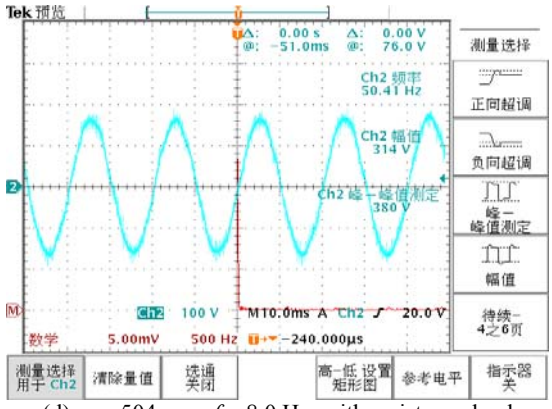

(d). n_r =504 rpm, f_c =8.0 Hz, with resistance load

Fig. 3 Voltage of BDFM power windings under different rotary speed and load condition

B. *Maximum wind power capture*

Fig.4 shows the relations among wind power, wind speed and rotary speed. Under different wind speed, the blade tip speed ratio λ of maximum power point is a constant. The principle of maximum power point tracking (MPPT) control is to adjust the rotary speed of wind turbine according to wind speed, and keep the wind turbine working at optimal blade tip speed ratio λ_{opt}. The dashed line in Fig.4 is the maximum power curve under different wind speed, and it's given as

$$P_{mopt} = \frac{1}{2} C_{p\max} \rho \pi R^2 \left(\frac{\omega_r R}{\lambda_{opt}}\right) \tag{2}$$

where, C_{pmax} is the maximum wind power coefficient, ρ is the air density, R is the radius of wind turbine, ω_r is the rotary speed of wind turbine.

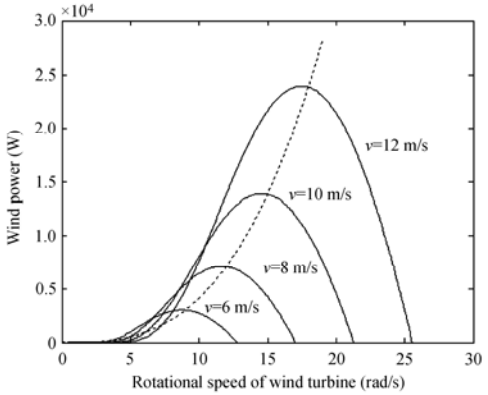

Fig.4 Relations between wind power captured and rotary speed under different wind speed

C. *Power decoupled control*

The BDFM is a time varying, nonlinear and strong coupled system, whose model is very complex (Fig.5) [3]. The power decoupled control is a difficulty in wind turbine control systems. The voltage-forced mode of the BDFM in the rotor speed d-q axis coordinate frame is given as [4]:

$$\begin{bmatrix} u_{qp} \\ u_{dp} \\ u_{qc} \\ u_{dc} \\ 0 \\ 0 \end{bmatrix} = \begin{bmatrix} r_p + L_{sp}p & 3\omega_r L_{sp} & 0 & 0 & M_c p & 3\omega_r M_p \\ -3\omega_r L_{sp} & r_p + L_{sp}p & 0 & 0 & -3\omega_r M_p & M_p p \\ 0 & 0 & r_c + L_{sc}p & \omega_r L_{sc} & -M_c p & \omega_r M_c \\ 0 & 0 & -\omega_r L_{sc} & r_c + L_{sc}p & \omega_r M_c & M_c p \\ M_p p & 0 & -M_c p & 0 & r_r + L_r p & 0 \\ 0 & M_p p & 0 & M_c p & 0 & r_r + L_r p \end{bmatrix} \begin{bmatrix} i_{qp} \\ i_{dp} \\ i_{qc} \\ i_{dc} \\ i_{qr} \\ i_{dr} \end{bmatrix} \tag{3}$$

where, r_p, L_{sp}, r_c, L_{sc}, r_r, L_r are the resistances and self-inductions of power winding, control winding, and rotor windings, respectively, and M_p, M_c are the inductions among power windings, control windings and rotor windings.

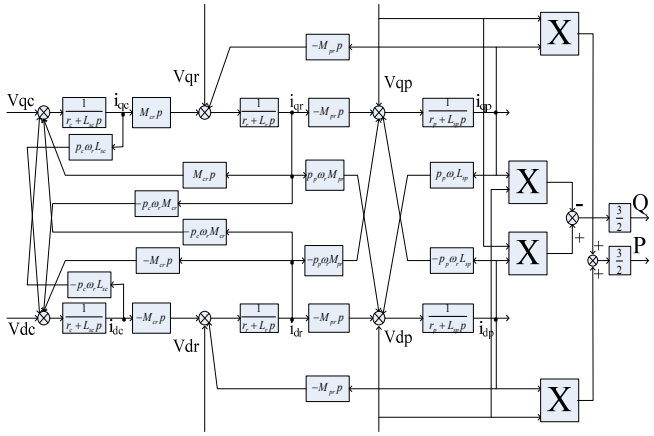

Fig. 5 Model of BDFM

Basing on (3), reference [5] and [6] developed the state space model as

$$\begin{bmatrix} \dot{x}_1 \\ \dot{x}_2 \\ \dot{x}_3 \\ \dot{x}_4 \end{bmatrix} = \begin{bmatrix} 0 & 1 & 0 & 0 \\ a_{21} & a_{22} & \omega_r a_{23} & -\omega_r \\ 0 & 0 & 0 & 1 \\ -\omega_r a_{23} & \omega_r & a_{21} & a_{22} \end{bmatrix} \begin{bmatrix} x_1 \\ x_2 \\ x_3 \\ x_4 \end{bmatrix} \quad (4)$$

$$+\frac{1}{k}\begin{bmatrix} 0 & 0 \\ 1 & 0 \\ 0 & 0 \\ 0 & -1 \end{bmatrix}\begin{bmatrix} u_{dc} \\ u_{qc} \end{bmatrix} + \begin{bmatrix} 0 & 0 \\ 1 & 0 \\ 0 & 0 \\ 0 & 1 \end{bmatrix}\begin{bmatrix} f_{dc} \\ f_{qc} \end{bmatrix}$$

where, $x_1 = \int i_{dr} dt$, $x_2 = i_{dr}$, $x_3 = \int i_{qr} dt$, $x_4 = i_{qr}$,

$$a_{21} = \frac{r_c}{M_c k} r_r,\ a_{22} = (L_r - \frac{M_p^2}{L_{sp}})\frac{r_c}{M_c k} + \frac{L_{sc}}{M_c k} r_r,$$

$$a_{23} = \frac{L_{sc}}{M_c k} r_r,\ k = (L_r - \frac{M_p^2}{L_{sp}})\frac{L_{sc}}{-M_c} + M_c,$$

$$f_{dc} = \sqrt{\frac{3}{2}}\frac{M_p V}{L_{sp} M_c k \omega_{1p}}\left[\left(4\omega_r - \omega_{1p}\right) L_{sc} \sin\theta_{pe} + r_c \cos\theta_{pe}\right],$$

$$f_{qc} = \sqrt{\frac{3}{2}}\frac{M_p V}{L_{sp} M_c k \omega_{1p}}\left[\left(\omega_{1p} - 4\omega_r\right) L_{sc} \cos\theta_{pe} + r_c \sin\theta_{pe}\right]$$

The active power and reactive power of power winding in the power winding synchronous rotary coordinate frame is given as

$$P_p = \frac{3}{2}(u_{qp}^{pe} i_{qp}^{pe} + u_{dp}^{pe} i_{dp}^{pe}) = -\frac{3}{2} V \frac{M_p x_4^{pe}}{L_{sp}} \quad (5)$$

$$Q_p = \frac{3}{2}(u_{qp}^{pe} i_{dp}^{pe} - u_{dp}^{pe} i_{qp}^{pe}) = \frac{3}{2L_{sp}} V \left[\sqrt{\frac{3}{2}}\frac{V}{\omega_p} - M_p x_2^{pe}\right] \quad (6)$$

The active power reference is set according to the MPPT curve given by (2), and the reactive power reference is set according to the requirement of power grid. Reference [6] applies auto disturbance rejection control (ACRC) [7] into the power decoupled control of BDFM. Fig.6 shows the diagram of control system, in which the convertor uses AC-AC matrix convertor [8]. Simulation results are shown in Fig.7 and Fig.8. In Fig.7, the reference of reactive power is constant and the wind speed step changes. The rotary speed of wind turbine changes according to the wind speed, and the power coefficient keeps at the maximum value, which means MPPT is achieved. In Fig.8, the wind speed is constant and the reference of reactive power is step changed. The reactive power tracks the reference quickly when the rotary speed and active power are almost unchanged, and the power coefficient is still kept at the maximum value. The ADRC effectively achieved the MPPT and power decoupled control of BDFM. Fig.7 (d) and Fig.8 (d) shows the output voltage of matrix convertor which is applied at control winding.

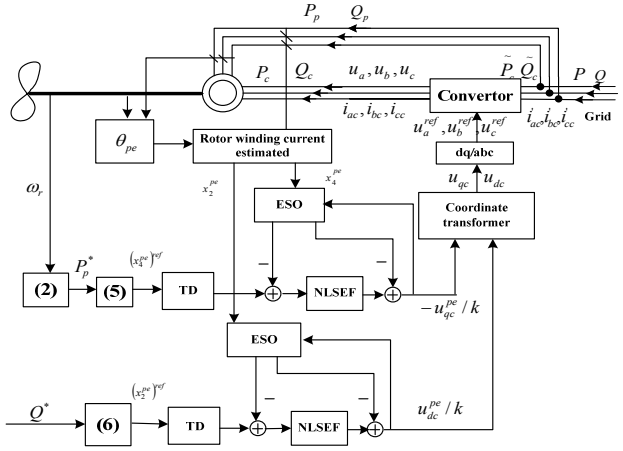

Fig.6 Power decoupled control diagram of the WECS with the BDFM

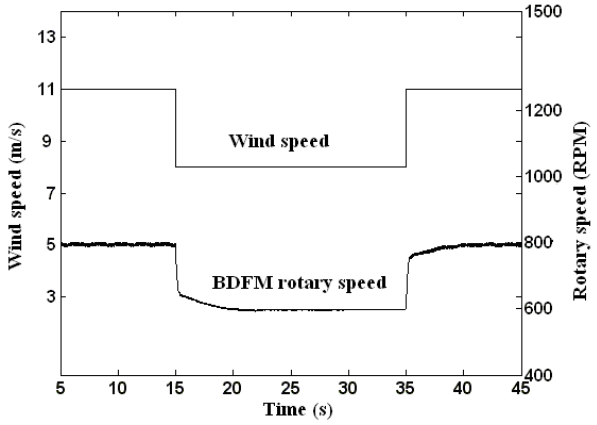

(a) Wind speed and BDFM rotary speed

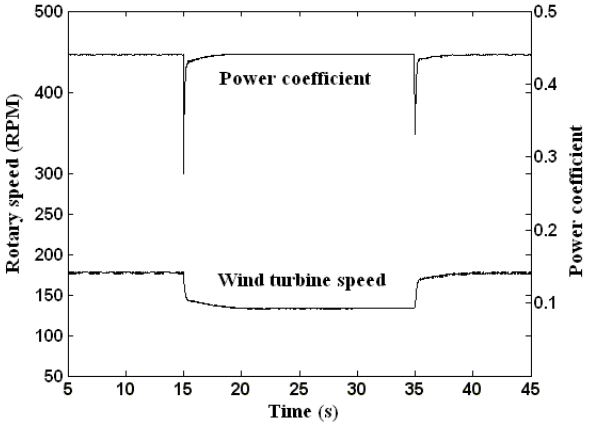

(b) Wind turbine rotary speed and power coefficient

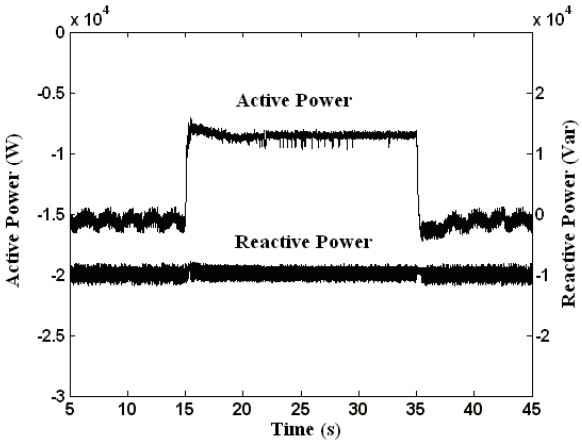

(c) Power output of the power windings

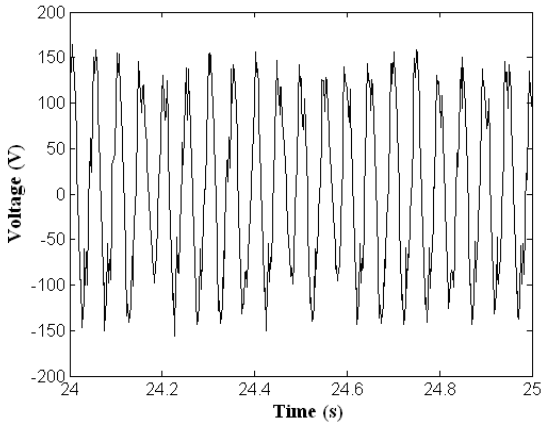

(d) Voltage output of the matrix converter

Fig.7 Response to step changed of wind speed

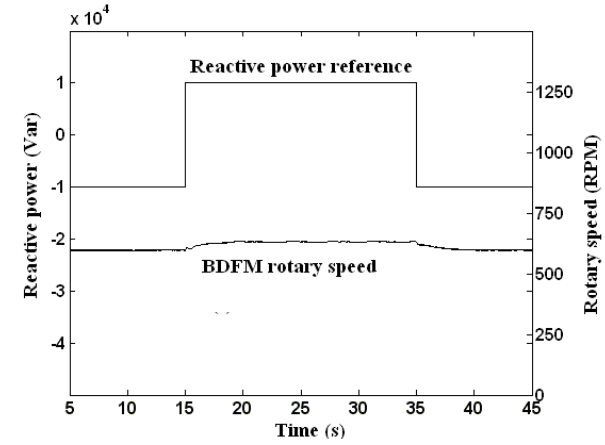

(a) Reactive power reference and BDFM rotary speed

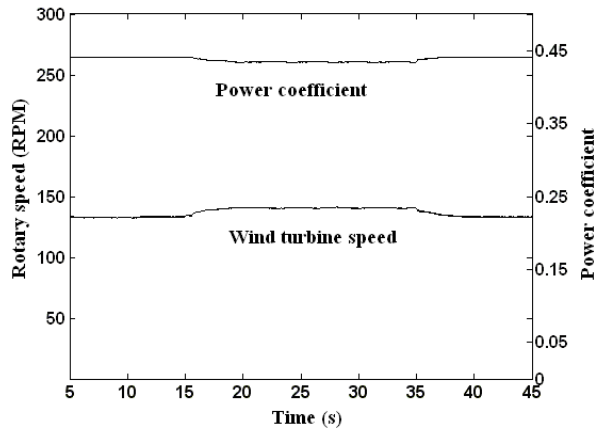

(b) Wind turbine rotary speed and power coefficient

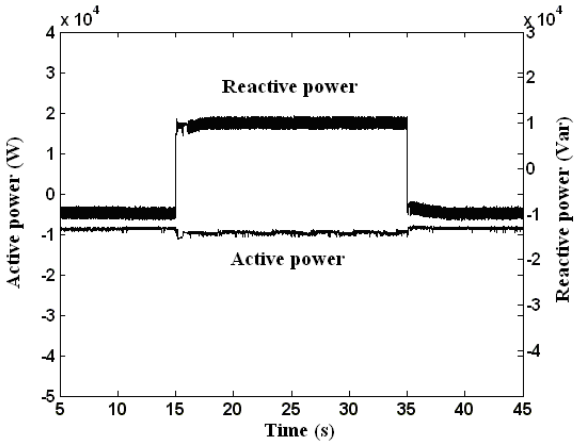

(c) Power output of the power windings

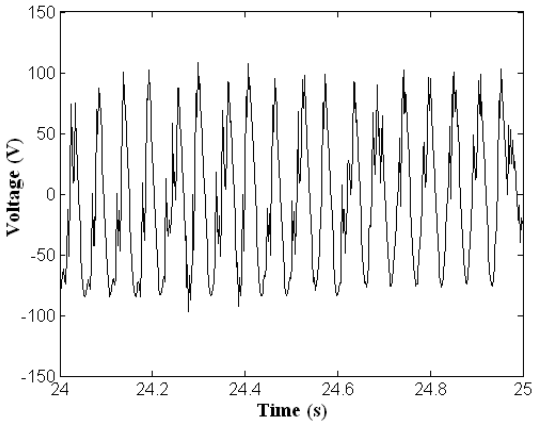

(d) Voltage output of the matrix converter

Fig.8 Response to step changed of reactive reference value

D. Pitch control

Torque control and pitch control can both limit the power capture of wind turbine when wind speed is above rated value. However, if only torque control is used, the generator has to offer large electromagnetic torque to reduce the rotary speed of wind turbine [9]. Large energy stored as rotor kinetic energy will transfer into power grid and lead to power fluctuation. Reference [10] present a pitch control method based on H-infinity control. The pitch angle of wind turbine is adjusted to keep the rotary speed and torque at rated value. The mechanical system nonlinear model of variable speed pitch control wind turbine is given as

$$\begin{cases} \dot{\omega}_r = -\dfrac{B_{ls}+K_r}{J_r}\omega_r + \dfrac{B_{ls}}{J_r n_g}\omega_g - \dfrac{K_{ls}}{J_r}\theta + \dfrac{1}{J_r}T_a \\ \dot{\omega}_g = \dfrac{B_{ls}}{J_g n_g}\omega_r + (\dfrac{K_g}{J_g} - \dfrac{B_{ls}}{J_g n_g^2})\omega_g + \dfrac{K_{ls}\theta}{J_g n_g} - \dfrac{1}{J_g}T_{em} \\ \dot{\beta} = -\dfrac{1}{T_\beta}\beta + \dfrac{1}{T_\beta}\beta_r \\ \dot{\theta} = \omega_r - \dfrac{\omega_g}{n_g} \end{cases} \quad (7)$$

When wind speed is 13m/s, the linearized model of system near equilibrium point is given as

$$\begin{bmatrix} \dot{\omega}_r \\ \dot{\omega}_g \\ \dot{\beta} \\ \dot{\theta} \end{bmatrix} = \begin{bmatrix} -137.43 & 22.3214 & -70.0741 & -1000 \\ 22.3214 & -4.97 & 0 & 223.2143 \\ 0 & 0 & -5 & 0 \\ 1 & -0.2232 & 0 & 0 \end{bmatrix} \begin{bmatrix} \omega_r \\ \omega_g \\ \beta \\ \theta \end{bmatrix} \quad \textbf{(8)}$$

$$+ \begin{bmatrix} 0 \\ 0 \\ 5 \\ 0 \end{bmatrix} u + \begin{bmatrix} 214.115 \\ 0 \\ 0 \\ 0 \end{bmatrix} v$$

The transfer function matrix of system is given as

$$\omega_g = P_2 u + P_1 w \tag{9}$$

where, $P_1 = \dfrac{4780s^2 + 71690s + 238970}{s^4 + 147.4s^3 + 1946.6s^2 + 8025.4s + 9261.8}$,

$$p_2 = \frac{-7821s - 78208}{s^4 + 147.4s^3 + 1946.6s^2 + 8025.4s + 9261.8}$$

The control problem can be described as a standard H-infinity control problem shown in Fig.9. The transfer function between input and output is given as

$$\begin{bmatrix} z_1 \\ z_2 \\ -\omega_g \end{bmatrix} = \begin{bmatrix} -W_e P_1 & -W_e P_1 \\ 0 & W_u \\ -P_1 & -P_2 \end{bmatrix} \begin{bmatrix} v \\ \beta_r \end{bmatrix} \tag{10}$$

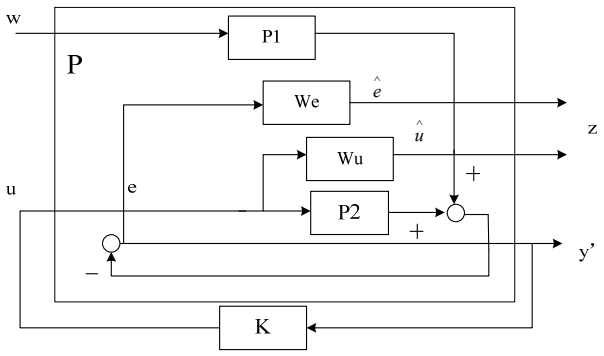

Fig.9 Standard H-infinity design diagram for power regulation

The weighting function W_e is chosen to keep the rotary speed of generator at rated value during steady state, and the weighting function W_u is used to limit the response speed of pitch angle to avoid saturation.

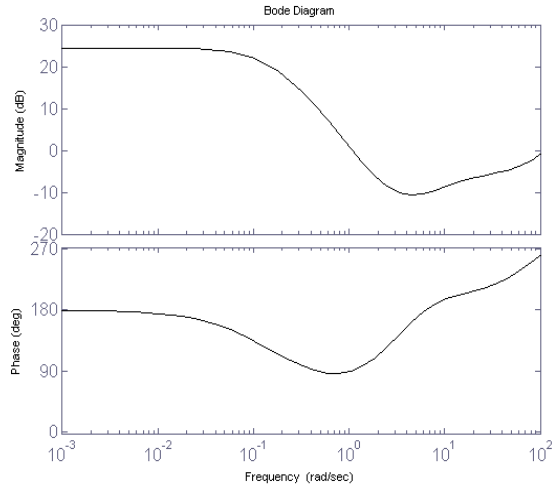

(a) Bode diagram of controller K_1

The weighting functions are chosen as (11), whose bode diagrams are shown in Fig.10.

$$W_u(s) = \frac{10s}{s+100} \quad , \quad W_e(s) = \frac{0.1(s+10)}{s+0.1} \tag{11}$$

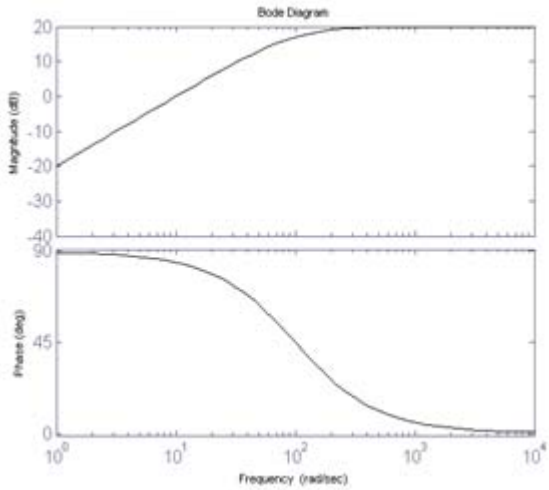

(b) Bode diagram of W_u

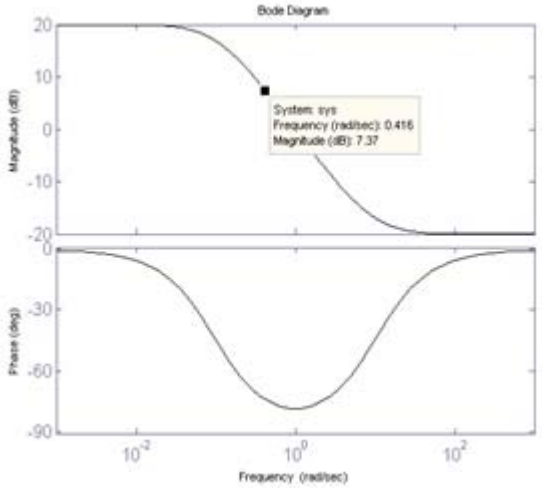

(c) Bode diagram of W_e

Fig.10 Bode diagrams of the functions

Simulation results in Fig.11 show that the pitch angle increases with wind speed, which keeps the rotary speed and capture power at rated value and hence achieves power limited control. Fig.12 shows the response of wind turbine with 5% error of rotary inertia, which verifies the robustness of controller.

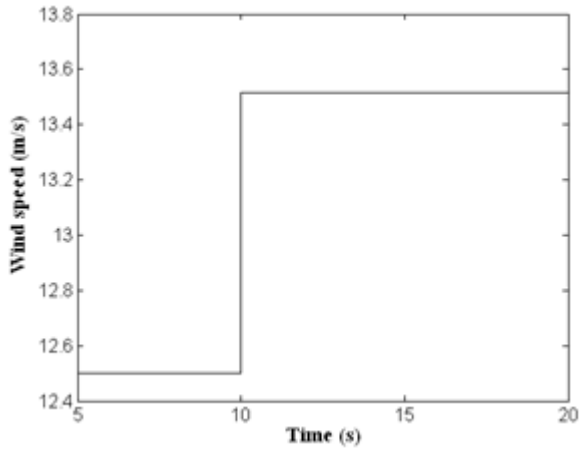

(a) Wind speed

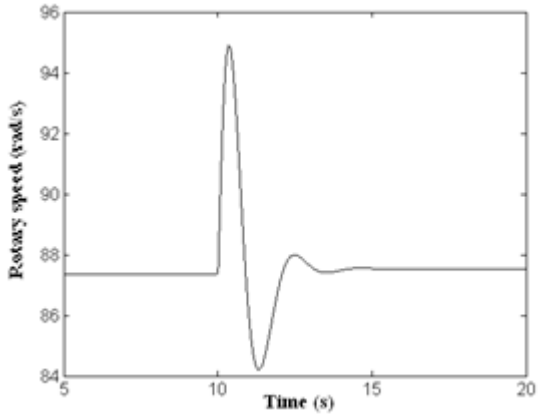

(b) Rotary speed of generator

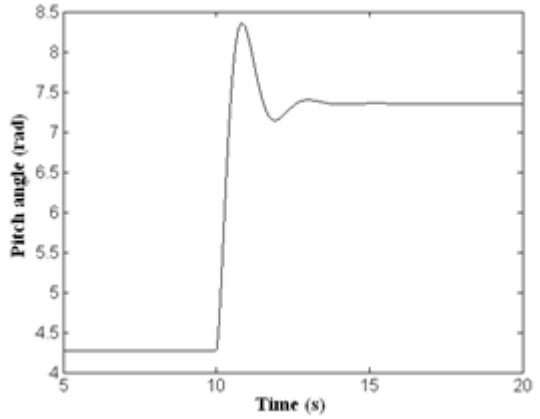

(c) Pitch angle

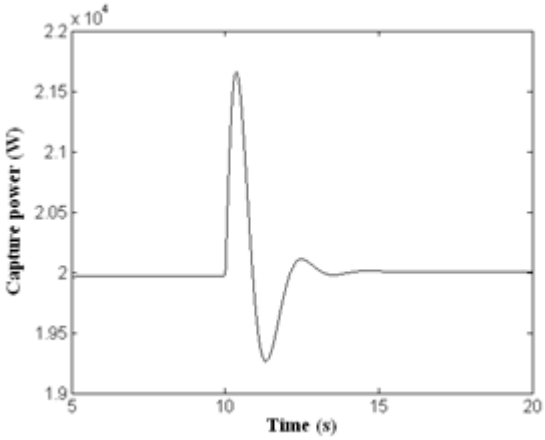

(d) Capture power

Fig.11 Dynamic response of wind turbine above rated wind speed

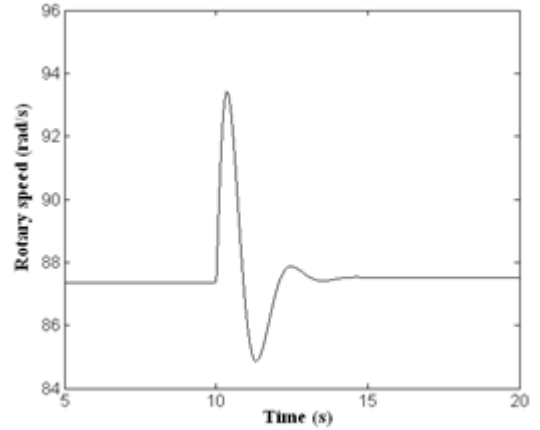

Fig.12 Rotary speed of generator with 5% error of rotary inertia

E. Low voltage ride through

The relations among rotor winding current and voltage of DFIG are given as

$$\begin{cases} \dfrac{di_{rd}}{dt} = \dfrac{u_{rd}}{\sigma L_r} - \dfrac{R_r i_{rd}}{\sigma L_r} + \dfrac{\omega_s \varphi_{rq}}{\sigma L_r} - \dfrac{L_m}{\sigma L_r L_s}\dfrac{d\varphi_{sd}}{dt} \\ \dfrac{di_{rq}}{dt} = \dfrac{u_{rq}}{\sigma L_r} - \dfrac{R_r i_{rq}}{\sigma L_r} - \dfrac{\omega_s \varphi_{rd}}{\sigma L_r} - \dfrac{L_m}{\sigma L_r L_s}\dfrac{d\varphi_{sq}}{dt} \end{cases} \quad (12)$$

Traditional control method based on ideal grid voltage always neglect the stator flux transient term in (12). When the grid voltage dips, the transient component in stator flux will induce large current in rotor winding, which may damage the exciting convertor [11]. Reference [12] introduces ADRC to combine with vector control (Fig.13). The influences of disturbances, including stator transient flux and generator parameter errors, are estimated and compensated by the extended state observer (ESO).

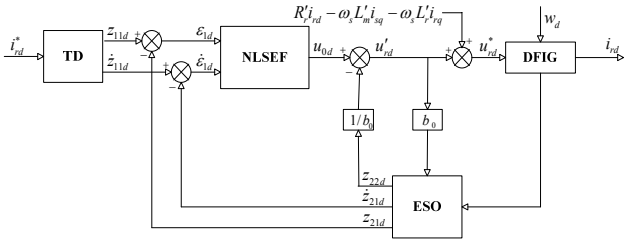

Fig. 13 ADRC of d-axis rotor current

The simulation results of traditional control and ADRC during grid voltage dip are compared in Fig.14. Because the ADRC scheme includes disturbances compensation, the voltage applied into rotor winding increases, which decreases the peak current of rotor winding. The ADRC scheme effectively avoids over current in rotor winding, and hence, protects the exciting convertor during grid voltage dip. Additional simulation results in [12] show excellent robustness of ADRC against generator parameter errors.

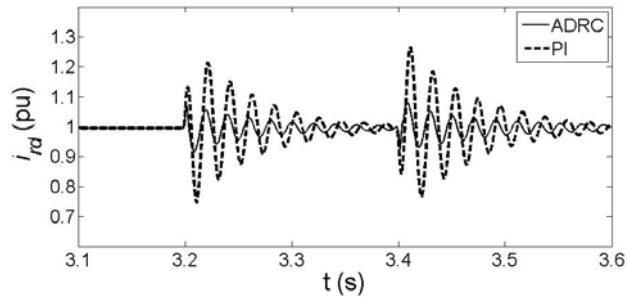

(a) d-axis rotor current

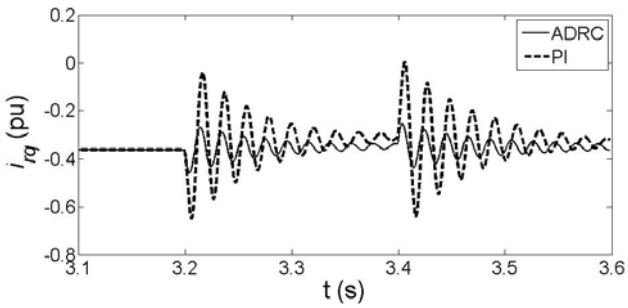

(b) q-axis rotor current

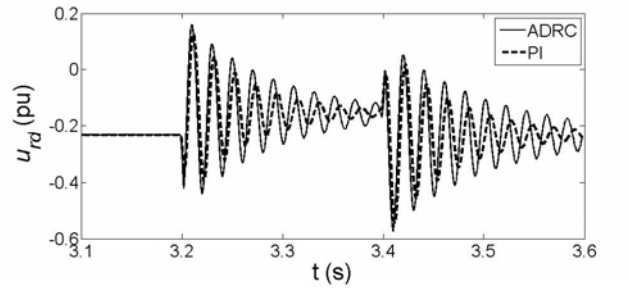

(c) d-axis rotor voltage

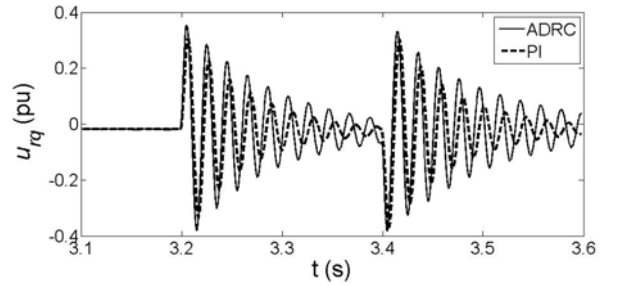

(d) q-axis rotor voltage

Fig. 14 Comparison of PI and ADRC control under grid voltage dip fault

F. Grid synchronization control

The control objective of grid synchronization is to control the stator direct and quadrature voltage to track the grid direct and quadrature voltage in the grid voltage reference frame, respectively, such that the stator voltage and grid voltage will have equal magnitude, frequency, and phase [13].

Cascaded control approaches are shown in Fig.15. The inner loop controls rotor current, and the outer loop minimizes the voltage differences between generator stator and power grid. The grid and stator line voltages of the DFIG are shown in Fig.16 (a) at rotor speed of 1400 rpm, and the corresponding direct and quadrature voltages are shown in Fig.16 (b). The stator voltage tracks the grid voltage rapidly and has its amplitude, frequency, and phase equalized to those of the grid voltage in several periods. The results are very similar at super-synchronous speed.

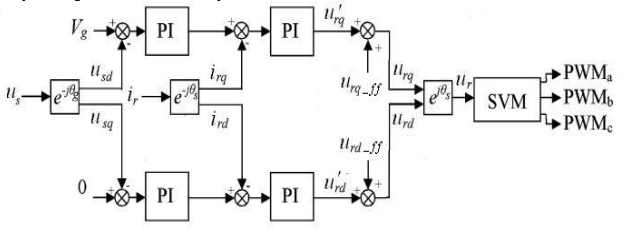

Fig.15 Control scheme of grid synchronization

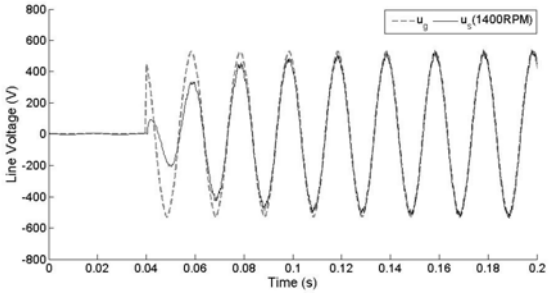

(a) Grid and stator line voltages

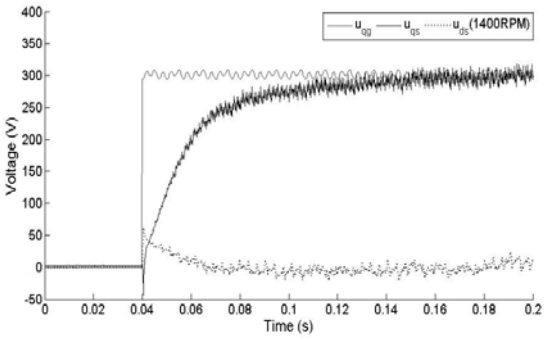

(b) Grid, stator direct and quadrature voltages

Fig. 16 Experiment results of grid synchronization

III. CONTROL TECHNOLOGIES IN PHOTOVOLTAIC GENERATION

A. Photovoltaic maximum power point tracking

Fig.17 shows a buck-boost DC/DC convertor for MPPT control of photovoltaic (PV) array [14].

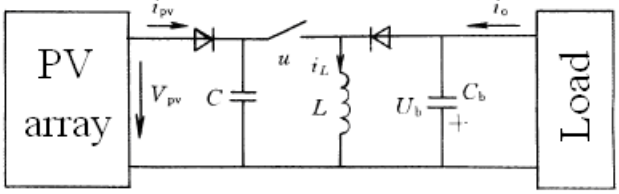

Fig.17 Photovoltaic generation system

Define u as the switching function of the switching component, $u=1$ means the switching is closed and $u=0$ means the switching is open circuit. The model of system is given as

$$\begin{cases} \dot{U}_{pv} = \dfrac{1}{C} i_{pv} - \dfrac{u}{C} i_L \\ \dot{i}_L = -\dfrac{1}{L} U_b + \dfrac{u}{L}(U_{pv} + U_b) \\ \dot{U}_b = \dfrac{(i_L - i_0)}{C_b} - \dfrac{u}{C_b} i_L \end{cases} \tag{13}$$

where, U_{pv} and i_{pv} is the terminal voltage and output current of PV array, respectively.

A MPPT control scheme of PV array based on sliding mode control is designed in [15]. The sliding surface is chosen as

$$S = \frac{\partial p_{pv}}{\partial U_{pv}} = (\frac{\partial i_{pv}}{\partial U_{pv}} U_{pv} + i_{pv}) \tag{14}$$

The switching control signal is chosen as

$$u = \begin{cases} 0 & S \geq 0 \\ 1 & S < 0 \end{cases} \tag{15}$$

Reference [15] proves that the system with controller satisfies the Lyapunov stability condition. Hence, the system can reach and finally settle in the sliding surface. The simulation result during light intensity step change is shown in Fig.18. p_{pv1} and U_{pv1} are the output power and terminal voltage of PV array with sliding mode control. p_{pv2} and U_{pv2} are the output power and terminal voltage of PV array with traditional comparative control scheme. The sliding mode control improves the response speed of MPPT.

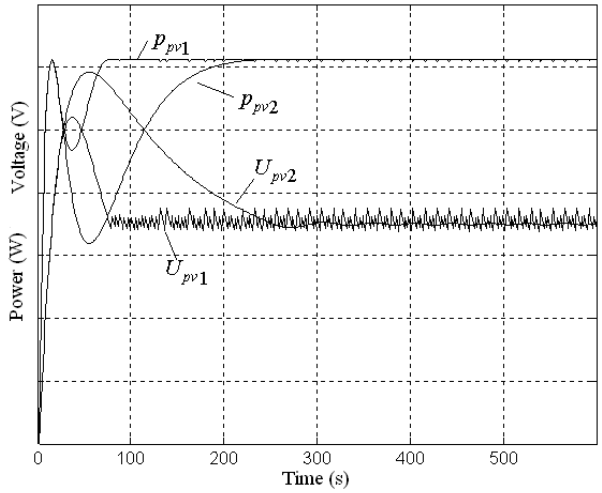

Fig.18 The terminal voltage and output power response of PV array with light intensity step changed

B. Photovoltaic array configuration optimization control

Reference [16] presents a configuration optimization control scheme for PV array. The principle is to change the PV batteries arrangement when the temperature and light intensity of the PV batteries have large different, and make sure that all the PV batteries works near the maximum power point (MPP), which will optimize the total output power of the whole PV array.

The basic principle is as follows

(1) The optimization terminal voltages of every PV pile at the maximum power point are calculated according to the measured temperature and light intensity. If the terminal voltage difference between two PV piles, such as U_1 and U_3, is larger than 1.5 Um, reconfiguration is necessary.

(2) If $(U_3 - U_1) \in ((n-0.5)U_{3m}, (n+0.5)U_{3m}]$, the reconfiguration method is as follow

If n is even, the configuration of array is changed as

$$\begin{bmatrix} U_1 \\ U_2 \\ U_3 \end{bmatrix} = \begin{bmatrix} NU_{1m} + (n/2-1)\,U + U_{3m} \\ NU_{2m} \\ (N+1-\mathrm{n})U_{3m} \end{bmatrix} \tag{16}$$

If n is odd, the configuration of array is changed as

$$\begin{bmatrix} U_1 \\ U_2 \\ U_3 \end{bmatrix} = \begin{bmatrix} NU_{1m} + (n-1)\;U/2 \\ NU_{2m} \\ (N+1-\mathrm{n})U_{3m} \end{bmatrix} \tag{17}$$

where, $n \in [2,N]$, and U is the parallel connection of two U_{3m} PV batteries.

(3) If $(U_1 - U_3) \in ((n-0.5)U_{1m}, (n+0.5)U_{1m}]$, the reconfiguration method is as follow

If n is even, the configuration of array is changed as

$$\begin{bmatrix} U_1 \\ U_2 \\ U_3 \end{bmatrix} = \begin{bmatrix} (N+1-\mathrm{n})U_{1m} \\ NU_{2m} \\ NU_{3m} + (n/2-1)U + U_{1m} \end{bmatrix} \tag{18}$$

If n is odd, the configuration of array is changed as

$$\begin{bmatrix} U_1 \\ U_2 \\ U_3 \end{bmatrix} = \begin{bmatrix} (N+1-\mathrm{n})U_{1m} \\ NU_{2m} \\ NU_{3m} + (n-1)U/2 \end{bmatrix} \tag{19}$$

where, $n \in [2,N]$ and U is the parallel connection of two U_{1m} PV batteries.

Simulation of a given illustration is carried out. Three PV piles mounted at different aspect of a building, such as east, south and west, have different temperature and light intensity at a moment. The temperature and light intensity is listed as 298K, 0.8kW/m^2; 301K, 0.95kW/m^2; 306K, 1.1kW/m^2. If the arrangement of the PV array is 33×3, then the power-voltage curves of three PV pile shown in Fig.19 are T_1, T_2, and T_3. T is the total power-voltage curve of the whole PV array. If traditional fixed array scheme is used, only the third PV pile works at MPP, and the other two PV pile both deviate from the MPP. The total output power of the PV array is 7501W.

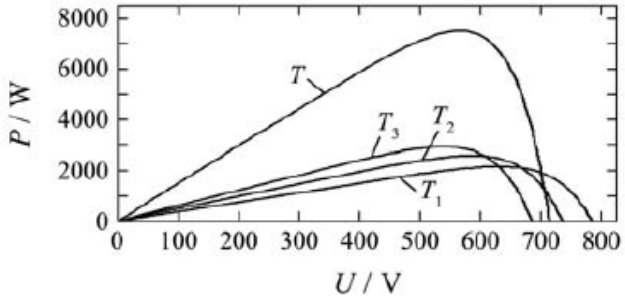

Fig.19 Power-voltage curves of PV pile with different conditions

As shown in Fig.19, the terminal voltage of three PV pile at the maximum power point are 613.8V, 573.2V and 557.6V. The terminal voltage difference between east pile and west pile satisfies $(U_1 - U_3) \in (2.5U_{1m}, 3.5U_{1m}]$, and hence the PV array should be rearranged according to (19). The result of configuration optimization is shown in Fig.20. In the new PV array after configuration optimization, only two batteries in the first pile don't work at the MPP and deviate from the MPP little. The total output power of the PV array is 7928W, which increase 5.69% before configuration optimization.

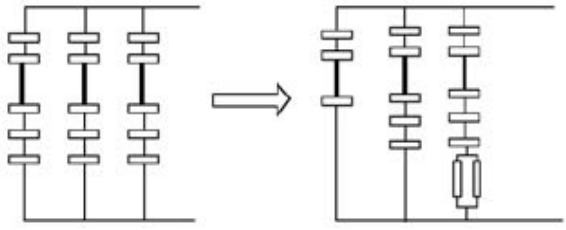

Fig.20 Configuration optimization of PV array

C. Grid-connected control for photovoltaic array

A PV gird-connected converter is shown in Fig.21 [17]. The system model neglecting high frequency switching dynamic is given as

$$\begin{cases} \dfrac{du_c}{dt} = -\dfrac{1}{R_L C}u_c - \dfrac{i_s}{Cu_c}u_a + \dfrac{1}{C}i_e \\ \dfrac{di_s}{dt} = -\dfrac{R}{L}i_s + \dfrac{1}{L}u_s - \dfrac{1}{L}u_a \end{cases} \qquad (20)$$

According to the nonlinear character of the grid-connected converter, an ADRC scheme is designed in [17], whose structure is shown in Fig.22.

Cascaded control approaches are used. The inner loop is current proportion control loop, which control the output current of the convertor to follow reference value. The grid voltage is considered as external disturbance, whose influence to the system is suppressed by the auxiliary feedback branch. The outer loop is voltage control loop, in which the DC side voltage is control by the ADRC. The output current of the PV array is considered as external disturbance, which is observed and compensated by the extension state observer (ESO).

The simulation results with traditional PI control scheme and proposed ADRC scheme are shown in Fig.23 and Fig.24, respectively. The overshoot of capacitor voltage and the inrush of current are suppressed by the ADRC scheme. Fig.25 shows that if the output power of PV is more than load, the phases of voltage and current of the convertor are the same and energy transfers from the system to grid. Contrarily, the phases are inversed and energy transfers from grid to the system. The convertor has excellent performance under both modes.

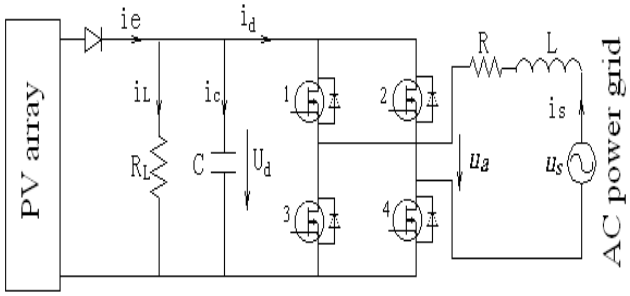

Fig.21 PV grid-connected convertor

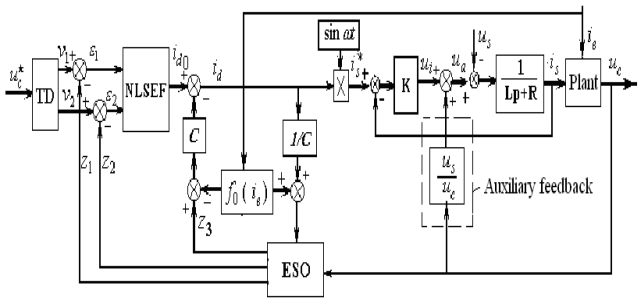

Fig.22 Control scheme of PV grid-connected convertor

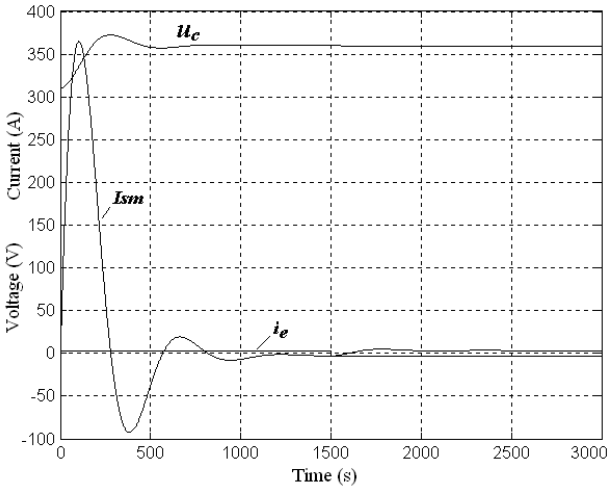

Fig.23 System response with PI control scheme

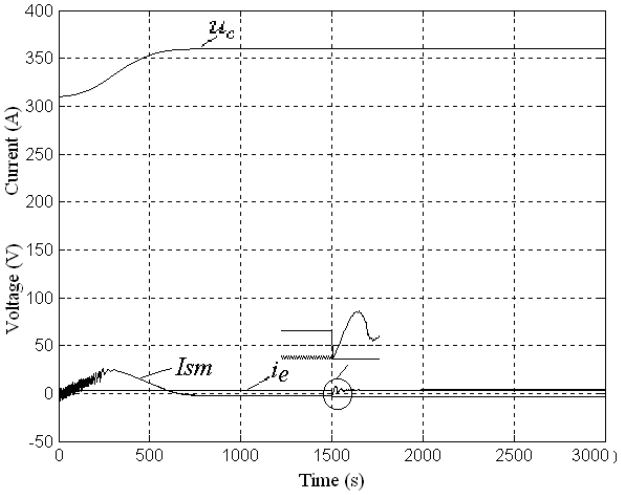

Fig.24 System response with ADRC scheme

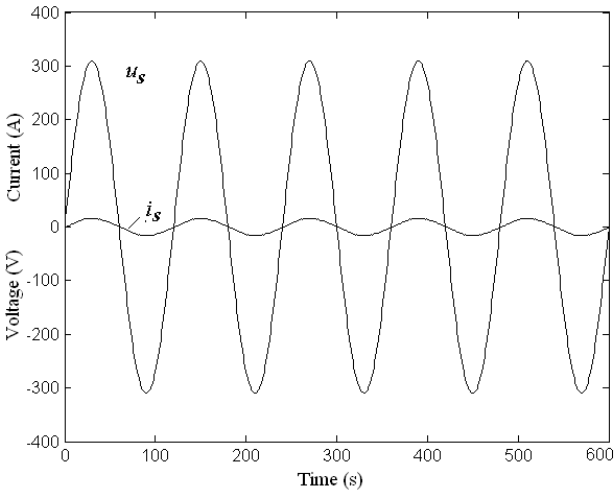

(a) PV output power is more than load

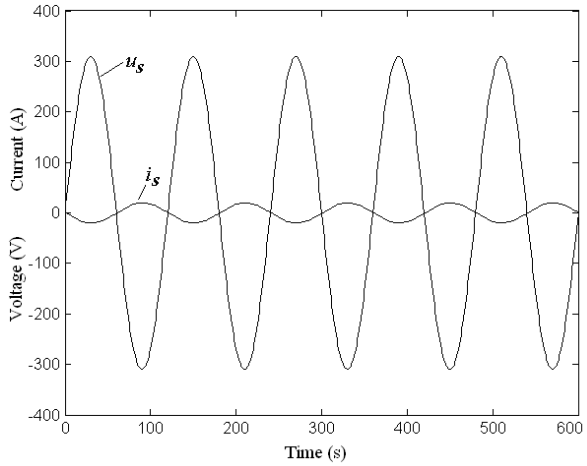

(b) PV output power is less than load

Fig.25 Output voltage and current of PV grid-connected convertor

The hardware experimental results are shown in Fig.26 and Fig.27. In Fig.26, the first waveform is with ADRC scheme and the second waveform is with PI control scheme. The experimental results are very similar with simulation results, which also verify the better performance of ADRC. Fig. 27 shows the voltage of grid and output current of convertor, whose phase are almost the same.

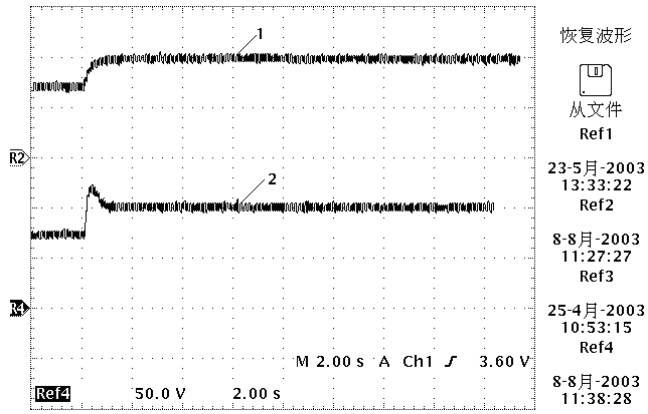

Fig.26 Experimental response of ADRC and PI

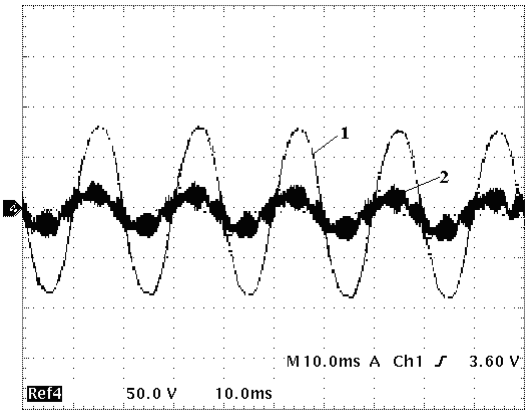

Fig.27 Grid voltage and convertor output current

IV. ENERGY MANAGEMENT SYSTEM

1. Wind Speed and power prediction

With a view to the randomicity of wind, the forecast of wind resource plays more and more important role in the scheduling system in wind power farm. Combination the forecast of wind speed and output power is a good way to improve the performance in scheduling of wind power farm. A new approach to forecast wind speed and output power were accomplished based on Box-Jenkins random time series theory [18].

Different experiments results are discussed based on different wind speed as follows.

Firstly, when the wind speed is changed gently, the prediction result and absolutely error are shown in the Fig.28 (a) and (b) respectively. Where, the blue line is the initial data from Shanwei Wind Power Farm， and the red one is the result of forecast. Absolute error (AE), relative error (RE) and mean absolute error (MAE) are calculated according to equation 21.

$$AE = y - \hat{y}$$
$$RE = \frac{y - \hat{y}}{y} \times 100\% \qquad (21)$$
$$MAE = \frac{1}{N}\sum_{i=1}^{N}\frac{|y_i - \hat{y}_i|}{y_i}$$

Where, y is truth value, $\hat{}$ means the value of forecast. From the Fig.28, the prediction results are good, and the MAE just hits 6.046%.

Secondly, when the wind speed is changed in a large scale, the prediction results are shown in Fig.29, and the MAE is 9.21%. The results show good performance of this algorithm, which can be used in wind power farm in future.

The output power of wind turbine is also accomplished by the same algorithm. The experiment results are shown in Fig.30. The MAE hits 16.62%.

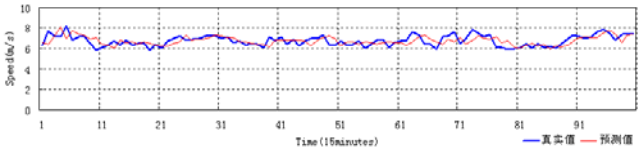

(a) Wind speed prediction

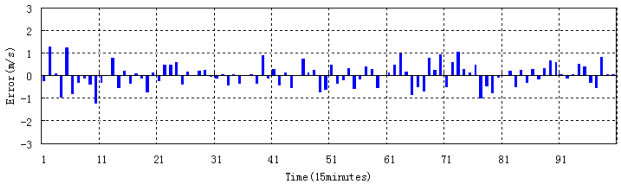

(b) Absolute error

Fig.28 Wind speed prediction in real time

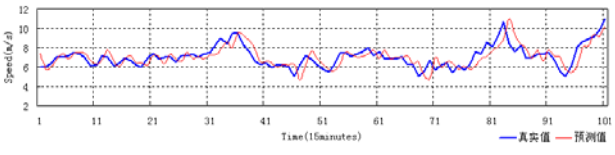

(a) Wind speed prediction

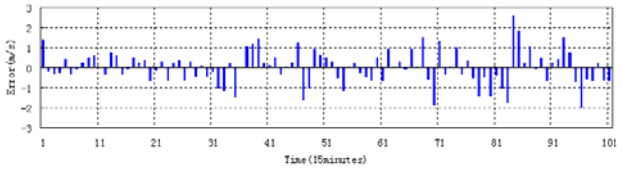

(b) Absolute error

Fig.29 Wind speed prediction

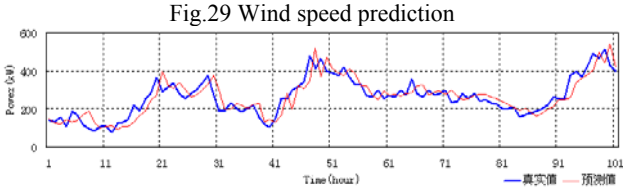

(a) Power prediction series

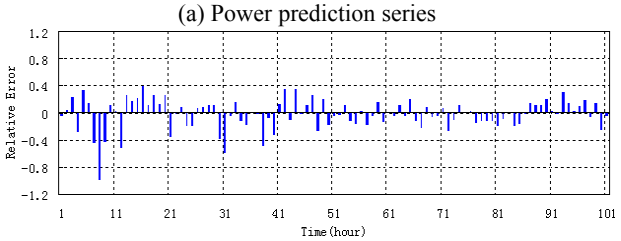

(b) Relative error in power prediction

Fig.30 Power prediction

2. Power Quality

Due to the intermittence and uncontrollable of RE, doubts to the power quality and stability of RE power system are the main hindrance to develop RE power system. As a result, evaluation and monitoring of power quality plays most important role in RE power system.

2.1. Power quality evaluation

According to IEEE-Std100-1992, we introduced six indexes of power quality in RE power, including Voltage Sags, Frequency Deviation, Voltage Fluctuation, Flicker, Waveform Distortion, and Three-phase Unbalanced [19]. Especially, power fluctuation is proposed with a view to the characteristics of RE，which be defined as follows.

$$\Delta P_n = \frac{P_{nt} - P_{(n-1)t}}{t} \times 100\% \tag{22}$$

$$D_P = \frac{P_{\max} - P_{\min}}{P_N} \times 100\% \tag{23}$$

Where, P is the output power, n is sampling number, t is sampling time. ΔP_n and D_P are the variable rate and amplitude rate of output power respectively. P_N is the root mean squares of all sampling data during sampling period, P_{max} and P_{min} are the maximum and minimum value.

Analytic hierarchy process (AHP) is adopted to obtain weight for each index as defined above. Then, to evaluate power quality of RE, a synthetic evaluation approach is proposed as follows, which combines probability and statistics with fuzzy mathematics.

Step 1, define evaluation period, $T=t$;

Step 2, each index is divided into m qualification ranks with step length as $\Delta q=x/m$. Where, $m\geq 10$，x is the limit value of each index according to national standard.

Step 3, summing the time when data locates in the same rank.

$$\tau(k) = \sum_{i=1}^{n} t_i \tag{24}$$

Where, t_i is the i time period when the absolute value of index locate in the rank k，n is the total number of times when the absolute value of index locate in the rank k.

Step 4, calculate the probability distribution of index at rank K, and then forming a 1×m matrix.

$$P_k = \tau(k)/T \tag{25}$$

$$R' = [p_1, \quad p_2, \quad p_3, \quad \cdots \quad p_m] \tag{26}$$

Step 5, integrate all the indexes' matrix into a 8×m matrix

$$R = [R_{VS} \quad R_{TPU} \quad R_{VF} \quad R_{WD} \quad R_{FD} \quad R_F \quad R_{\Delta P} \quad R_{DP}]' \tag{27}$$

where, R_Z, R_T, R_V, R_X, R_P, R_S, R_B, R_G are matrix of voltage sags, three-phase unbalanced, voltage fluctuation, harmonic distortion, frequency deviation, flicker, power fluctuation ΔP and D_P respectively.

Step 6, Adopt analytic hierarchy process (AHP) to obtain weight for each indexes, and let assessment value as $V=W\times R$, where,

$$W = [W_{VS} \quad W_{TPU} \quad W_{VF} \quad W_{WD} \quad W_{FD} \quad W_F \quad W_{\Delta P} \quad W_{DP}]$$

the suffixes are defined as step 5.

Step 7, Apply Additive Weight Method in V, get the assessment value.

$$V' = \sum_{k=1}^{m} kV_k \Big/ \sum_{k=1}^{m} V_k \tag{28}$$

Where, V' is the final assessment result.

2.2. A portable power quality analyzer

We developed a new portable power quality analyzer based on dual CPU (DSP+ARM). Data process and communication are divided into two parts with different CPU. DSP is designed to charge data process and sent information to ARM via SCI communication port. ARM is designed to compute, display and storage the data from DSP. Further more, ARM also supplies another communication port which can joint into monitor net based on optical Ethernet network as shown in Fig.31 [20].

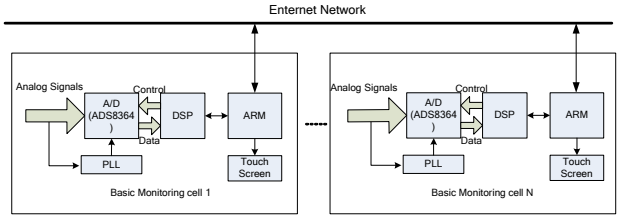

Fig.31 The power quality monitoring network based on optical fiber ethernet.

The simultaneous Data Acquisition System (DAS) is based on synchronized Phase Lock Loop (PLL), which can track the frequency of the input signal. And Fast Fourier Transform Spectrum Analysis (FFTSA) is introduced into the system to improve the accuracy and reliability greatly. The chip ADS8364, a multi-channel simultaneous chip, measures three-phase voltage and current simultaneously. So, it analyzes the power quality with high accuracy. This is a great development of the general equipment which just evaluates the single phase power quality.

A series of experiments have been done with this power quality analyzer in Shanwei Red Bay, Guangdong province. From the results of practically application, the power quality analyzer not only obtained parameters from power quality from several wind turbines, also synchronously completed the initial analysis, assessment and certification of data. A typical experiment results as shown in Fig.32, including voltage and current waveforms, voltage harmonic data, current harmonic data, and voltage etc. Now, further testing is under way, we believe the performance of the Power Quality Analyzer will be improved step by step.

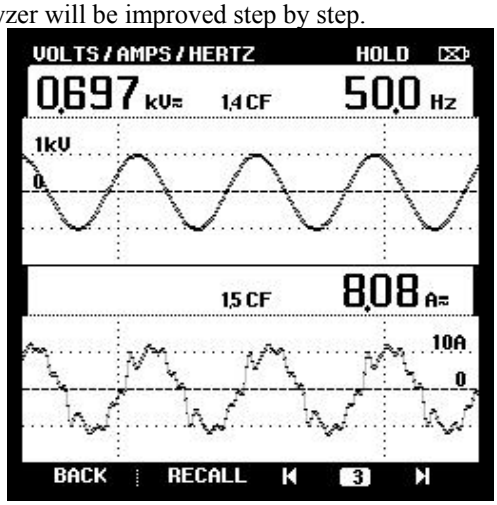

(a) The wind turbine voltage and current of phase A

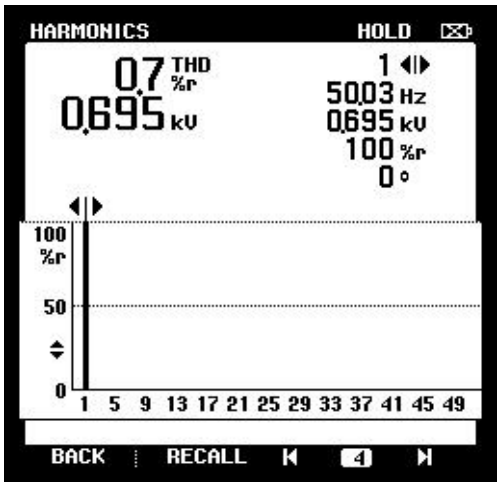

(b) The wind turbine voltage harmonics of phase A

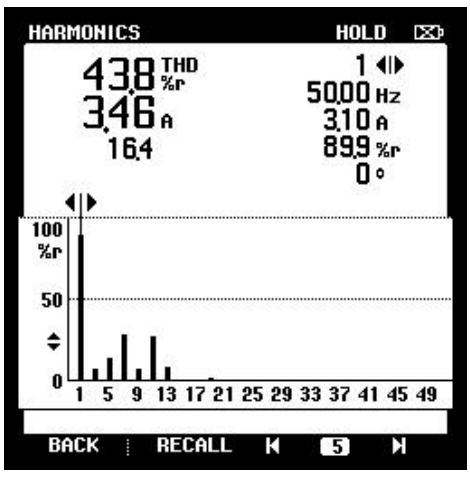

(c) The wind turbine current harmonics of phase A

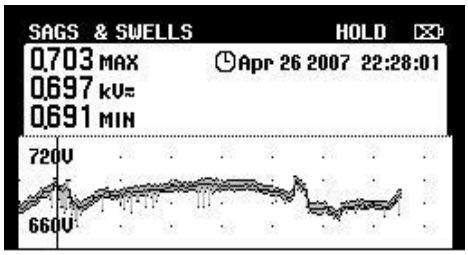

(d) Voltage fluctuation of UBC

Fig.32 Experiment results of the portable power quality analyzer

3. Energy Management System based on Multi-Agent Technology

A novel energy management system is developed based on hybrid multi-agent (MAS) technology. The multi-agent technology is the evolution of the classical distributed technology with specific characteristics, which provided new abilities in controlling complex system. According to the characteristics of renewable energy power system, an intelligent hybrid control system is proposed to embed in the intelligent agent. "Hybrid" stands for that the system plays continuous control algorithm in a certain mode, and plays discrete control strategy in mode transitions when external environment changed. Agents with layered architectures are designed to present RE source utility as shown in Fig.33 [21]. There are five layers, including monitoring layer, union mission planning layer, negotiating and cooperating layer, motion control layer, continue controlling layer, as well as executing and performance evaluating module.

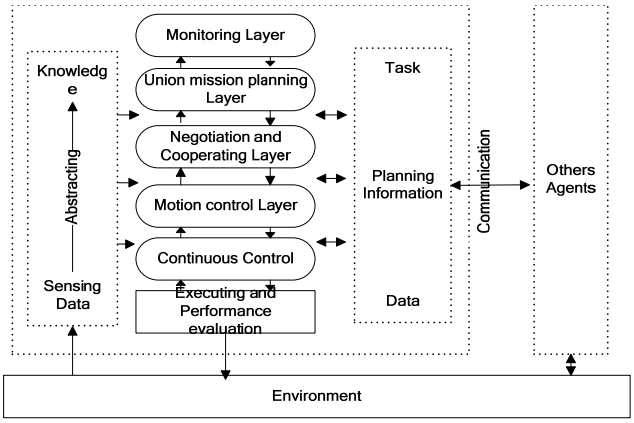

Fig.33 The framework of Agent

The agent can be defined as follows [22]

$$\text{Agent}=\{\text{ID},\text{G},\text{S},\text{IP},\text{CC},\text{I},\text{E},\text{ST},\text{A},\text{R},\text{K}\} \quad (29)$$

Where, these elements are defined as follows: Agent-ID, Goal, Sensor, Information Processing，Communicating and Cooperating，Integrated Processing, Effect, State, Ability, Rule database, Domain Knowledge. Especially, states define a discrete operation mode {S1, S2, S3, S4} to present the characterization of the node at macrostructure. S4 stands for operation. S3 stands for the hot stand-by. S2 stands for the cold stand-by. S1 stands for the maintenance outage. Fig.34 shows the relationship of the different mode.

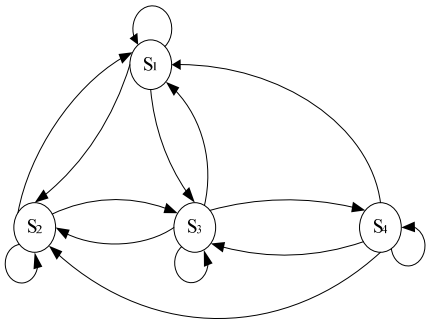

Fig.34 The transition of different mode

According to the demands and requirements of RE power system, the station of optimization and decision-making is shown as follows [23]

$$\min \frac{\sum_i tC_{Wi}P_{Wi}(t)+\sum_j tC_{PVj}P_{PV\,j}(t)}{\sum_i tP_{Wi}(t)+\sum_j tP_{PV_j}(t)} \quad (t=1,2,...,T) \quad (30)$$

s.t. $\sum_i P_{W_i}(t)+\sum_j P_{PV_j}(t)-P_L(t)\pm P_{BAT}(t)=0$,

$Q_f=\sum_{i=1}^{8} W_i Eq_i \geq C$, $P_{BAT-\mathrm{MIN}} \leq P_{BAT} \leq P_{BAT-\mathrm{MAX}}$

Where, C_{Wi}, C_{PVj}, P_{Wi}, P_{PVj} are the per-cost and output power of wind turbines and PV arrays respectively, Q_f is the synthetic power quality index.

Based on the objectives mentioned above, the continuous control is implemented by reinforcement learning algorithm. And two cooperation methods are proposed. One is master-slave model based on improved contract-net protocol, the other is totally distributed model based on Petri net and cooperative task planning algorithm.

Energy management in RE power system is distributed and complex. The MAS not only provide perfect framework closing to the real system, but also integrate other AI techniques. The energy management system based on MAS meet the requirement about distribution, heterogeneity, openness, hybrid, cooperation and autonomous.

Nowadays, Micro-grid is a new concept in RE research filed. It is a generation system composed of low-voltage distribution networks, small modular generation devices and loads connected to them. It can also be regarded as a small scale grid based on distributed generation devices, to manage the supply and demand of local energy. Currently, it has become one of the hottest research issues in renewable energy field. The energy management system based on Multi-Agent will become one of main development directions of micro-grid.

V. CONCLUSION

The Environment protection is the most important problems in the countries' sustainable development. Energy should be more "environment friendly" and achieve "zero emission" by applying RE as power sources. Researches on energy management play a significant role in the process. This article mainly introduces the research efforts on control technologies in distributed generation system based on renewable energy by the New Energy Research Center of South China University of Technology, which includes wind energy generation, photovoltaic generation, and energy management system. For the intact purpose, some achievements by other researchers are referred.

ACKNOWLEDGMENT

The work described in this article was fully supported by the National Natural Science Foundation of China under Grant. 60534040.

REFERENCES

[1] J. Wu, S.Z. Chen, and J.H. Yang, "Control on green energy source and ecologic environment", Asian Power Electronic Journal, Vol. 1, No. 1, 2007, pp. 36-41.

[2] J.H. Yang, "Research on Wind Energy Conversion System and Control with Brushless Doubly-Fed Generator", Ph.D. thesis, South China University of Technology, China, 2006.

[3] J. Wu, S.Z. Chen, and D. Liu, "Control and Power Electronics Technology in Renewable Energy", SCIENCE IN CHINA SERIES E-TECHNOLOGICAL SCIENCES, Vol. 51, No. 6, 2008, pp. 702-712.

[4] R.Q. Li, "Dynamic modeling, simulation and stability analysis of brushless doubly fed machines", Ph.D. thesis, Oregon State University, American, 1991.

[5] X.Y. Zhang, J. Wu, and J.H. Yang, "Decoupled power control with sliding mode for brushless doubly-fed machine", Acta Energiae Solaris Sinica, Vol. 28, No. 1, 2007, pp. 68-73.

[6] X.Y. Zhang, "Modeling and control of wind energy conversion system with brushless doubly-fed machine", Ph.D. thesis, South China University of Technology, China, 2007.

[7] J.Q. Han, "From PID technique to active disturbance rejection control technique", Control Engineering, Vol. 3, No. 3, 2002, pp. 13-18.

[8] J. Wu, Z.H. Shi, J.H. Yang, and Y.R. Chen, "Simulation of Matrix Converter Based on Direct Torque Control", Journal of South China University of Technology (Natural Science Edition), Vol. 34, No. 4, 2006, pp. 47-55.

[9] S.Z. Chen, J. Wu, G.X. Yao, and J.M. Yang, "Power Limitation Control of Wind Turbine System Based on Differential Geometry Theory" Control Theory & Applications, Vol. 25, No. 2, 2008, pp. 336-340.

[10] X.Y. Zhang, J. Wu, J.M. Yang, and J. Shu, "H-infinity robust control of constant power output for the wind energy conversion system above rated wind", Control Theory & Applications, Vol. 25, No. 2, 2008, pp..

[11] J.B. Hu, D. Sun, and Y.K. He, "Modeling and control of DFIG wind energy generation system under grid voltage dip", Automation of Electric Power Systems, Vol. 30, No. 8, 2005, pp. 21-26.

[12] S.Z. Chen, J. Wu, and M. Liu, "Low voltage ride through control of DFIG wind energy generation system", Acta Energiae Solaris Sinica, (Accepted for publication).

[13] K.C. Wong, S.L. Ho, and K.W.E. Cheng, "Direct voltage control for grid synchronization of doubly-fed induction

generators", Electric Power Components and Systems, Vol. 36, No. 9, 2008, pp. 960-976.
[14] M. Zhang, "Research of wind and solar PV hybrid generating control system", Ph.D. thesis, South China University of Technology, China, 2004.
[15] M. Zhang, and J. Wu, "Application of Slide Technology in PV MPPT System", Transactions of China electro technical society, Vol. 20, No. 3, 2005, pp. 90-93.
[16] C.A. Cen, M. Zhang, and L.Q. Wang, "Control of the configuration optimization for photovoltaic array", Control Theory & Applications, Vol. 25, No. 2, 2008, pp. 364-366.
[17] M. Zhang, and J. Wu, "Control system of renewable energy connected grid based on the auto-disturbances rejection control technology", Control Theory & Applications, Vol. 22, No. 4, 2005, pp.583-587.
[18] Liu, "Research on Distributed Wind-Photovoltaic Hybrid Power Management System", Ph.D. thesis, South China University of Technology, China, 2008.
[19] Y.W. Ma, Y.R. Chen, and J. Zeng, "Analysis and evaluation on the electric power quality of wind farm", Control Theory & Applications, Vol. 25, No. 2, 2008, pp 307-310.
[20] Y. Zhang, J. Zeng, S.W. Wang, and X.M. Yu, "A Portable Power Quality Monitoring System for Wind Power Generation System", Control Theory & Application, Vol. 25, No. 1, 2008, pp. 163-166.
[21] Liu, J. Wu Jie, J. Zeng, H.X. Guo, and X.M. Yu, "Planning of Distributed Generating Management Based on Multi-Agent System", Control Theory & Application, Vol. 25, No. 1, 2008, pp. 151-154.
[22] J. Zeng, J. Wu, J.F. Liu, and L.M. Gao, "An Agent-based Approach to Renewable Energy Management in Eco-building", IEEE International Conference on Sustainable Energy Technologies, 2008, Nov, pp. 46-50.
[23] X.M. Yu, J. Zeng, H.X. Guo, and D. Liu, "Distributed Wind-PV System based on Multi-Agent and Petri Nets", Control Theory & Applications, Vol. 25, No. 2, 2008, pp. 353-356.